Analytical and computational study of the ideal full two-fluid plasma model and asymptotic approximations for Hall-magnetohydrodynamics

B. Srinivasan[a] and U. Shumlak
Aerospace and Energetics Research Program, University of Washington, Seattle, Washington 98195, USA

(Received 28 April 2011; accepted 23 August 2011; published online 28 September 2011)

The 5-moment two-fluid plasma model uses Euler equations to describe the ion and electron fluids and Maxwell's equations to describe the electric and magnetic fields. Two-fluid physics becomes significant when the characteristic spatial scales are on the order of the ion skin depth and characteristic time scales are on the order of the ion cyclotron period. The full two-fluid plasma model has disparate characteristic speeds ranging from the ion and electron speeds of sound to the speed of light. Two asymptotic approximations are applied to the full two-fluid plasma to arrive at the Hall-MHD model, namely negligible electron inertia and infinite speed of light. The full two-fluid plasma model and the Hall-MHD model are studied for applications to an electromagnetic plasma shock, geospace environmental modeling (GEM challenge) magnetic reconnection, an axisymmetric Z-pinch, and an axisymmetric field reversed configuration (FRC). © *2011 American Institute of Physics*. [doi:10.1063/1.3640811]

I. INTRODUCTION

The ideal full two-fluid plasma model[1] results directly from taking moments of the Vlasov equation for electrons and ions. The moment series can be truncated by assuming Maxwellian velocity distributions, which provides five moment equations. Though this model is seeing more frequent use recently,[2–5] it is more common to apply asymptotic approximations to arrive at reduced plasma models, for example, Hall-MHD or ideal MHD.[6–10] The two-fluid plasma model reduces to the Hall-MHD model when electron inertia is assumed negligible and speed of light is assumed infinite. However, other reduced plasma models can be derived by independently applying each asymptotic approximation.

The ideal full two-fluid plasma model is studied in this paper and is compared to reduced plasma models. Asymptotic approximations, namely negligible electron inertia and infinite speed of light, are applied independently to study the effect of the approximations on the dispersion relation. When both asymptotic approximations are applied simultaneously, the more commonly used Hall-MHD model is obtained. The full and asymptotically approximated two-fluid plasma models are explored analytically and computationally. Analytical dispersion relations are studied for each of these models. Simulations are performed using the full two-fluid plasma model and Hall-MHD for applications of an electromagnetic plasma shock, geospace environmental modeling (GEM challenge) magnetic reconnection, an axisymmetric Z-pinch, and an axisymmetric field reversed configuration (FRC) to explore the physics captured by each of these models. The code WARPX (Washington approximate Riemann plasma)[11,12] developed at the University of Washington is used for all the simulations in this paper.

The paper is outlined as follows. Section II describes the ideal full two-fluid plasma model. Section III applies the asymptotic approximations independently and simultaneously, and presents analytical dispersion relations describing the reduced plasma models. Section IV briefly describes the numerical method used for the simulations presented in the paper. Section V presents the applications of the full two-fluid plasma model and Hall-MHD to study the physics, accuracy, and computational efficiency of the models when using an explicit time-integration scheme. Discussions are presented in Sec. VI.

II. IDEAL FULL TWO-FLUID PLASMA MODEL

The full two-fluid plasma model is described by a complete set of Euler equations for the ions, a complete set of Euler equations for the electrons, and a complete set of Maxwell's equations to evolve the electric and magnetic fields. The source terms couple the fluid and field variables. Writing the fluid equations in balance law form gives

$$\frac{\partial \rho_s}{\partial t} + \nabla \cdot (\rho_s \mathbf{u}_s) = 0, \tag{1}$$

$$\frac{\partial \rho_s \mathbf{u}_s}{\partial t} + \nabla \cdot (\rho_s \mathbf{u}_s \mathbf{u}_s + p_s \mathbf{I}) = \frac{\rho_s q_s}{m_s}(\mathbf{E} + \mathbf{u}_s \times \mathbf{B}), \tag{2}$$

$$\frac{\partial \varepsilon_s}{\partial t} + \nabla \cdot ((\epsilon_s + p_s)\mathbf{u}_s) = \frac{\rho_s q_s}{m_s}\mathbf{u}_s \cdot \mathbf{E}, \tag{3}$$

where subscript, s, denotes electron or ion species, q_s and m_s are the species charge and mass. ρ_s is the mass density, $\mathbf{u}_s$ is the velocity, and p_s is the isotropic pressure of each species. $\mathbf{E}$ is the electric field and $\mathbf{B}$ is the magnetic field. The energy, ϵ_s, is defined as

$$\epsilon_s \equiv \frac{p_s}{\gamma - 1} + \frac{1}{2}\rho_s u_s^2. \tag{4}$$

[a]Electronic mail: srinbhu@u.washington.edu. Present address: Applied Mathematics and Plasma Physics, Los Alamos National Laboratory, Los Alamos, New Mexico 87545, USA.

The source terms of Eq. (2) contain the Lorentz forces on the electrons and ions. These source terms couple the fluid equations to the electromagnetic terms of Maxwell's equations. The Lorentz force acts as a body force on the electrons and ions.

Maxwell's equations are used to evolve the electric and magnetic fields using Faraday's law and Ampere's law described by

$$\frac{\partial \mathbf{B}}{\partial t} + \nabla \times \mathbf{E} = 0, \tag{5}$$

$$\frac{1}{c^2}\frac{\partial \mathbf{E}}{\partial t} - \nabla \times \mathbf{B} = -\mu_0 \mathbf{J}. \tag{6}$$

Additional divergence constraints are required.

$$\nabla \cdot \mathbf{E} = \frac{\varrho_c}{\varepsilon_0}, \tag{7}$$

$$\nabla \cdot \mathbf{B} = 0. \tag{8}$$

The current density and charge density are defined by the fluid variables as

$$\mathbf{J} \equiv \sum_s \frac{q_s}{m_s}\rho_s \mathbf{u}_s, \tag{9}$$

$$\varrho_c \equiv \sum_s \frac{q_s}{m_s}\rho_s. \tag{10}$$

If the initial fields satisfy the divergence constraints, then the fields evolved by Eqs. (5) and (6) will mathematically preserve the divergence constraints. However, divergence errors can develop in the numerical solution. Solving Eqs. (7) and (8) additionally leads to an over-specified system of equations. Hence, the perfectly hyperbolic Maxwell's equations[13] are used to evolve the electric and magnetic fields while maintaining the divergence constraints

$$\frac{\partial \mathbf{B}}{\partial t} + \nabla \times \mathbf{E} + \gamma \nabla \Psi = 0, \tag{11}$$

$$\frac{1}{c^2}\frac{\partial \mathbf{E}}{\partial t} - \nabla \times \mathbf{B} + \chi \nabla \Phi = -\mu_0 \mathbf{J}, \tag{12}$$

$$\frac{1}{\chi}\frac{\partial \Phi}{\partial t} + \nabla \cdot \mathbf{E} = \frac{\varrho_c}{\varepsilon_0}, \tag{13}$$

$$\frac{1}{\gamma c^2}\frac{\partial \Psi}{\partial t} + \nabla \cdot \mathbf{B} = 0. \tag{14}$$

In Eqs. (13) and (14), Φ and Ψ are the scalar error correction potentials for the divergence of $\mathbf{E}$ and for the divergence of $\mathbf{B}$, respectively. As the error correction coefficients, χ and γ, increase, the divergence constraints are recovered. For many problems, the error correction coefficients can be set to unity such that the errors are propagated out of the domain at the speed of light. This is often a sufficient condition; however, for some problems, additional divergence correction is required to accurately capture the evolution of the electromagnetic waves. In such situations, increasing the error correction coefficients leads to a more restrictive time step than the speed of light.

Analyzing the dispersion of characteristic waves provides a means of comparing various plasma models. The dispersion diagrams are computed by assuming the form $q(\mathbf{x}, t) = e^{i(\omega t - \mathbf{kx})}$, where ω is the frequency and k is the wave number, and linearizing the equations using this form. Figure 1 shows the dispersion diagrams for parallel propagation using the ideal full two-fluid plasma model. The

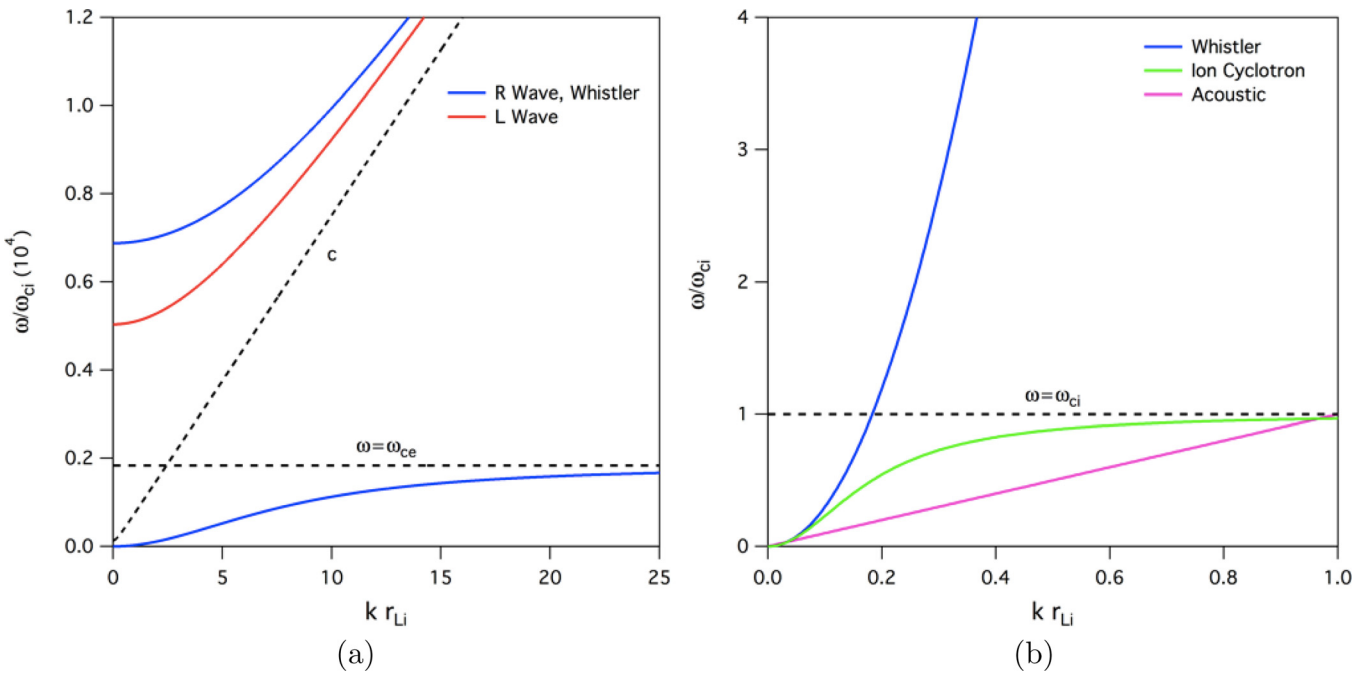

FIG. 1. (Color online) Parallel propagation dispersion relation of ω vs k for the two-fluid plasma model. Plot (a) shows R- and L-mode waves and right plot shows the low-frequency branch of the R-mode wave, the whistler wave, that has an asymptote at the electron cyclotron frequency. Plot (b) is an expanded scale of plot (a) to show the whistler wave, the ion cyclotron wave, and the ion acoustic wave.

R-mode and the L-mode waves are shown. Of particular interest is the whistler wave which is a part of the low-frequency spectrum of the R-mode wave. The whistler wave asymptotes to a resonance at the electron cyclotron frequency. The reason for choosing only the parallel propagation for all the dispersion diagrams presented here is to study the evolution of the whistler wave as the asymptotic approximations are applied. The whistler wave propagates parallel to the magnetic field.

For the ideal two-fluid plasma model, the characteristic speeds in the system are the fluid speeds of sound and the speed of light. The numerical method used to solve the two-fluid plasma model needs to be capable of resolving the physics in the presence of such disparate characteristic speeds. Furthermore, the characteristic frequencies in the system include the electron and ion plasma frequencies and the electron and ion cyclotron frequencies. All the speeds and frequencies must be resolved in the system to capture full two-fluid physics when using an explicit time-integration scheme. The explicit time step is described by

$$\Delta t = \min\left(\mathrm{CFL}\frac{\Delta x}{c}, \frac{0.1}{\omega_{pe}}, \frac{0.1}{\omega_{ce}}, \frac{0.1}{\omega_{pi}}, \frac{0.1}{\omega_{ci}}\right), \tag{15}$$

where c is the light speed, and

$$\omega_{ps} = \sqrt{\frac{n_s q_s^2}{\varepsilon_0 m_s}} \text{ and } \omega_{cs} = \frac{q_s B}{m_s} \tag{16}$$

are the plasma and cyclotron frequencies. CFL is the Courant condition for stability, and the factor of 0.1 is used to ensure that the frequencies are accurately resolved. Since $\omega_{pe} > \omega_{pi}$ and $\omega_{ce} > \omega_{ci}$, the explicit time step is given by

$$\Delta t = \min\left(\mathrm{CFL}\frac{\Delta x}{c}, \frac{0.1}{\omega_{pe}}, \frac{0.1}{\omega_{ce}}\right). \tag{17}$$

Exploring the canonical form of the momentum equation and taking the curl of that to obtain generalized vorticity,[14]

$$\frac{\partial \Omega_{\mathbf{s}}}{\partial t} - \nabla \times \mathbf{u_s} \times \Omega_s = -\nabla H, \tag{18}$$

$$H = \frac{\mathbf{u}_s^2}{2} + \frac{\phi}{m_s} + \int \frac{dp_s}{\rho_S}, \tag{19}$$

where $\Omega = \nabla \times \mathbf{p}$ is the generalized vorticity with $\mathbf{p}$ being the canonical momentum, ϕ is the electrostatic potential, and s is the species. In the two-fluid picture, the presence of electron mass allows the generalized vorticity to be retained for the electron fluid as well. As explored in the following sections, two-fluid effects become important when small spatial and temporal scales become significant with respect to the system scales. The full two-fluid plasma model allows generation of local magnetic fields due to small-scale ion as well as electron fluid motions. The electron generalized vorticity is only present as a conserved quantity when electron inertia is retained.

The full two-fluid plasma model is valid for simulations involving electron demagnetization due to the inclusion of electron inertia. Electron inertia allows the electrons to break the frozen-in flux condition. The two-fluid model is also valid in regimes where the ion Larmor radius is much smaller than the scale-length of interest as well as when the ion Larmor radius is much larger than the scale-length of interest. For large ion Larmor radii, single-fluid models are no longer relevant since the Larmor radius is assumed to be negligible in the single-fluid regime. To appropriately include effects of anisotropic pressure, finite Larmor radius effects need to be included and higher moments of the Vlasov equation need to be taken to explore this regime.

III. ASYMPTOTIC APPROXIMATIONS

Two asymptotic approximations are commonly applied to the full two-fluid plasma model described previously to obtain the reduced plasma models. These approximations are negligible electron inertia and infinite speed of light. Perfect charge neutrality follows from the infinite light speed approximation. In this section, each asymptotic approximation is applied independently and the resulting dispersion relations are studied. Applying both approximations together gives the Hall-MHD model.

A. Negligible electron inertia

Since the ions are more massive than the electrons, electron inertia is neglected in a majority of plasma fluid models. Neglecting electron inertia reduces the electron momentum equation described in Eq. (2) to the generalized Ohm's law,

$$n_e q_e \mathbf{E} = \nabla p_e - \mathbf{J}_e \times \mathbf{B}, \tag{20}$$

where $\mathbf{J}_e = -n_e e \mathbf{u}_e$, $q_e = -q_i = -e$. This approximation also eliminates the kinetic energy term in the electron energy described by Eq. (4).

The dispersion diagram for parallel propagation when only neglecting electron inertia in the full two-fluid plasma model is shown in Fig. 2. The ion cyclotron wave asymptotes to a resonance at the ion cyclotron frequency. The speeds of the whistler wave and the additional wave (wave 2) asymptote at the speed of light. Wave 2 has a cutoff at $\frac{\omega_{pi}^2+\omega_{ci}^2}{\omega_{ci}}$ and asymptotes to the light wave. The whistler wave no longer has a resonance and also asymptotes to the light wave.

B. Infinite speed of light

The infinite speed of light approximation is used to eliminate high frequency electromagnetic waves, so the regime of interest lies in the lower frequency plasma waves. This approximation is achieved by assuming that the permittivity of free space vanishes thus implying an infinite speed of light. Applying this approximation eliminates the displacement currents from Ampere's law in Eq. (12) and results in

$$\mathbf{J} = \frac{1}{\mu_0}\nabla \times \mathbf{B}, \tag{21}$$

such that $\mathbf{J} = \mathbf{J}_i + \mathbf{J}_e$.

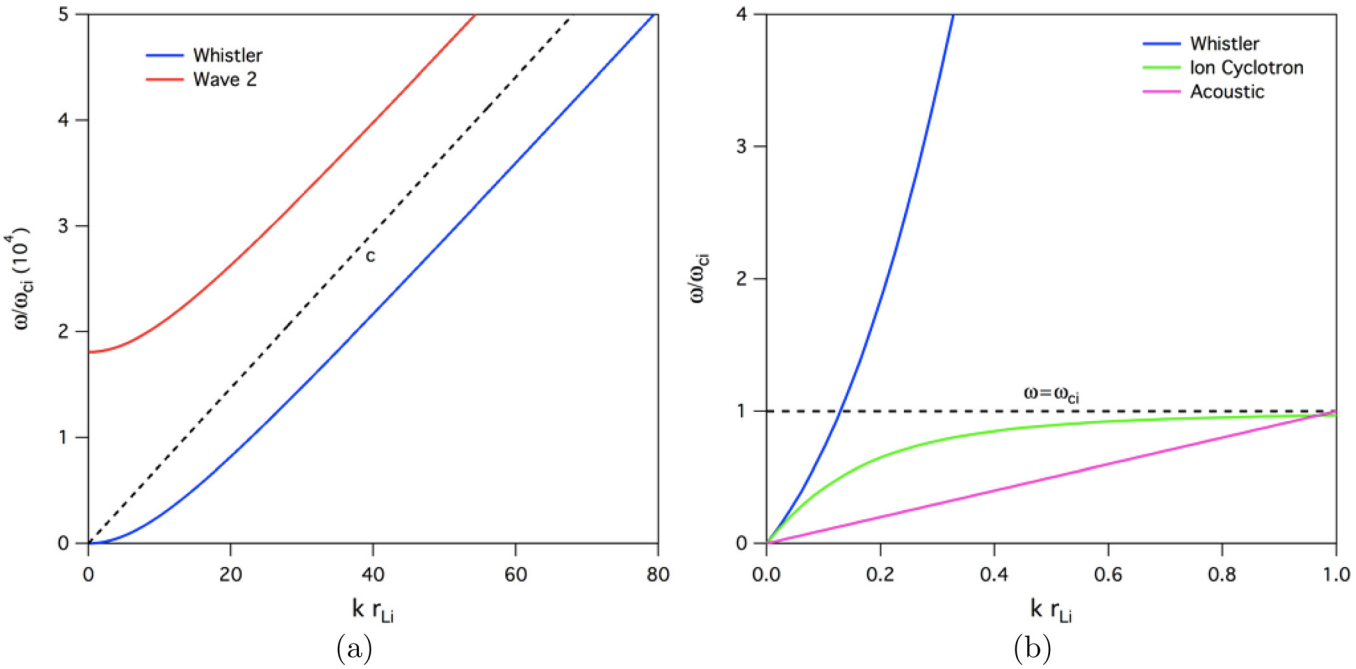

FIG. 2. (Color online) Parallel propagation dispersion relation of ω vs k when electron inertia is ignored in the two-fluid plasma model. The dashed black line represents the speed of light and is included for scale. Plot (b) has an expanded scale to show the whistler wave, the ion cyclotron wave, and the ion acoustic wave. The whistler wave reaches an asymptote at the speed of light. "Wave 2" is an additional wave of the dispersion relation that has an asymptote at the speed of light.

The dispersion diagram for parallel propagation when only assuming infinite light speed in the full two-fluid plasma model is shown in Fig. 3. Perfect charge neutrality is automatically implied through the mathematics of this approximation from Eq. (7) since $\varepsilon_0 \to 0$. The parallel dispersion relations for the infinite light speed assumption yield a whistler wave that retains the resonance at the electron cyclotron frequency and an ion cyclotron wave that retains the resonance at the ion cyclotron frequency. The high frequency R- and L-mode waves do not appear in this reduced model since $\varepsilon_0 \to 0$ eliminates the ion and electron plasma frequencies as well as the speed of light.

C. Reduction to the Hall-MHD model

Applying both of the above approximations gives the Hall-MHD model.[6] In the Hall-MHD model, the electron momentum equation reduces to the generalized Ohm's law, Ampere's law reduces to the form described in Eq. (21), and the electron continuity equation is eliminated due to charge neutrality. The Hall-MHD model is described by a complete set of Euler equations for ions, the generalized Ohm's law, an electron energy equation, Faraday's law, and the low-frequency Ampere's law (given by Eq. (21)).

A hyperbolic divergence cleaning method similar to the previously described perfectly hyperbolic Maxwell's equations is used for the Hall-MHD model.[13,15] The Hall-MHD model implemented here is described by

$$\frac{\partial \rho_i}{\partial t} + \nabla \cdot [\rho_i \mathbf{u}_i] = 0, \tag{22}$$

$$\frac{\partial \rho_i \mathbf{u}_i}{\partial t} + \nabla \cdot [\rho_i \mathbf{u}_i \mathbf{u}_i + p_i \mathbf{I}] = n_i e \mathbf{E} + \mathbf{J}_i \times \mathbf{B}, \tag{23}$$

$$\frac{\partial \epsilon_i}{\partial t} + \nabla \cdot [(\epsilon_i + p_i)\mathbf{u}_i] = \mathbf{J}_i \cdot \mathbf{E}, \tag{24}$$

$$\frac{\partial \epsilon_e}{\partial t} + \nabla \cdot [(\epsilon_e + p_e)\mathbf{u}_e] = \mathbf{J}_e \cdot \mathbf{E}, \tag{25}$$

$$n_e e \mathbf{E} = \frac{\rho_i}{m_i} e \mathbf{E} = \mathbf{J}_e \times \mathbf{B} - \nabla p_e, \tag{26}$$

$$\mathbf{J}_e = \frac{1}{\mu_0} \nabla \times \mathbf{B} - \mathbf{J}_i, \tag{27}$$

$$\frac{\partial \mathbf{B}}{\partial t} + \nabla \times \mathbf{E} + \nabla \Psi = 0, \tag{28}$$

$$\frac{\partial \Psi}{\partial t} + \Gamma^2 \nabla \cdot \mathbf{B} = -\zeta \Psi. \tag{29}$$

$\mathbf{J}_e$ is obtained from Eq. (21). Here, Γ is the speed at which the divergence of $\mathbf{B}$ errors is propagated out of the domain and ζ provides dissipation for the divergence errors. To obtain a perfectly hyperbolic divergence correction formulation, ζ is often assumed to be zero, so the error is swept out of the domain without dissipation similar to the implementation for the full two-fluid plasma model. Due to charge neutrality resulting from $\varepsilon_0 \to 0$, divergence of $\mathbf{E}$ errors are not an issue for the Hall-MHD model.

The dispersion diagram for parallel propagation for the Hall-MHD model is shown in Fig. 4. Figure 4 shows that the whistler wave frequency in the Hall-MHD model grows quadratically without bound in regimes where $\omega \sim \omega_{ci}$ and $k \sim 1/\delta_i$, where the ion skin depth is $\delta_i = c/\omega_{pi} = v_A/\omega_{ci} = r_{Li} c_{si}/v_A$ and the ion Larmor radius is r_{Li}. $c_{si}/v_A \approx 0.5$ is used in the dispersion diagrams. The quadratically growing frequency produces a whistler wave speed that increases without bound with

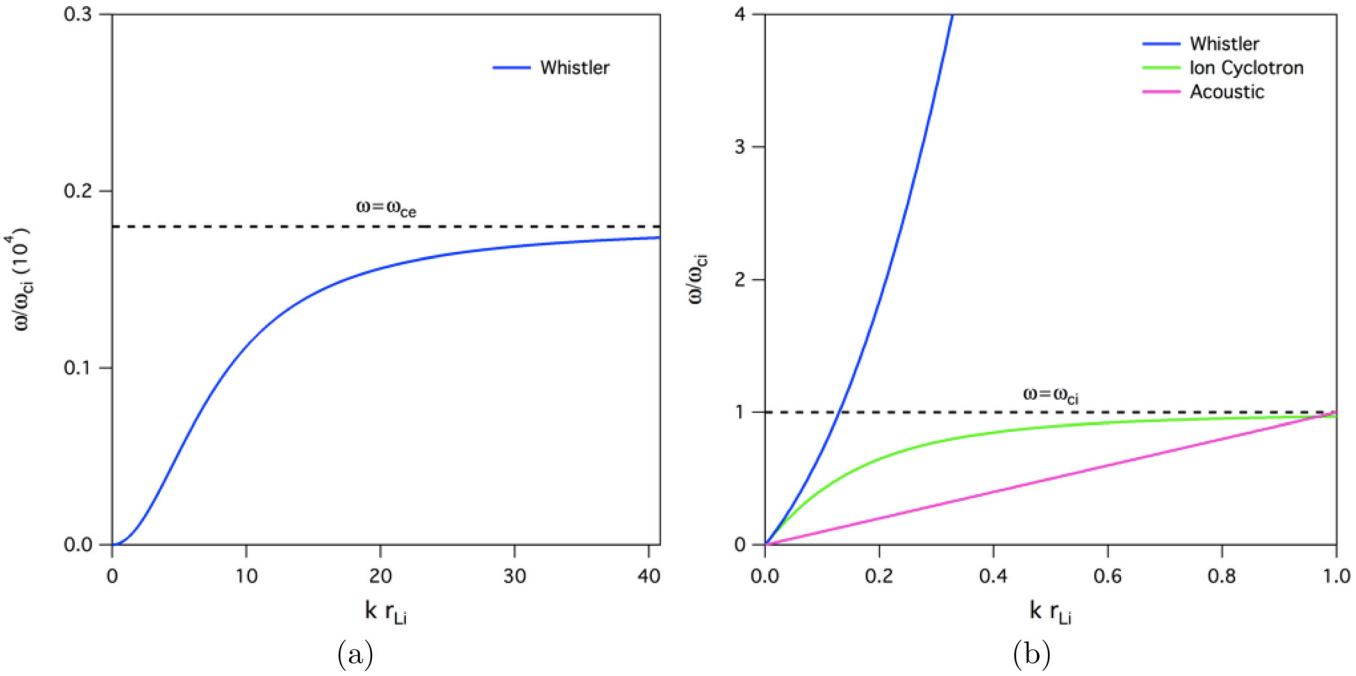

FIG. 3. (Color online) Parallel propagation dispersion relation of ω vs k when speed of light is assumed to be infinite in the two-fluid plasma model. Plot (a) shows the whistler wave that has an asymptote at the electron cyclotron frequency. Plot (b) has an expanded scale to show the whistler wave, the ion cyclotron wave, and the ion acoustic wave.

increasing wave number. If $k \ll 1/\delta_i$ $(\omega \ll \omega_{ci})$, the dispersion diagram resembles that of ideal-MHD and is only described at the origin of Fig. 4. This is more easily seen by examining the analytical dispersion relation for parallel propagation for the Hall-MHD model,[16]

$$\omega = \frac{1}{2}\omega_{ci}\delta_i^2 k^2 + \sqrt{v_A^2 k^2 + \frac{1}{4}\omega_{ci}^2\delta_i^4 k^4}, \tag{30}$$

where v_A is the Alfvén velocity. For $k \ll 1/\delta_i (\omega \ll \omega_{ci})$, the Alfvén wave dispersion relation varies linearly with k and resembles ideal-MHD. However, for sufficiently large k, the whistler wave becomes

$$\omega = \omega_{ci}\delta_i^2 k^2. \tag{31}$$

Therefore, for a regime where $k \gtrsim 1/\delta_i (\omega \gtrsim \omega_{ci})$, the whistler wave grows quadratically without bound.

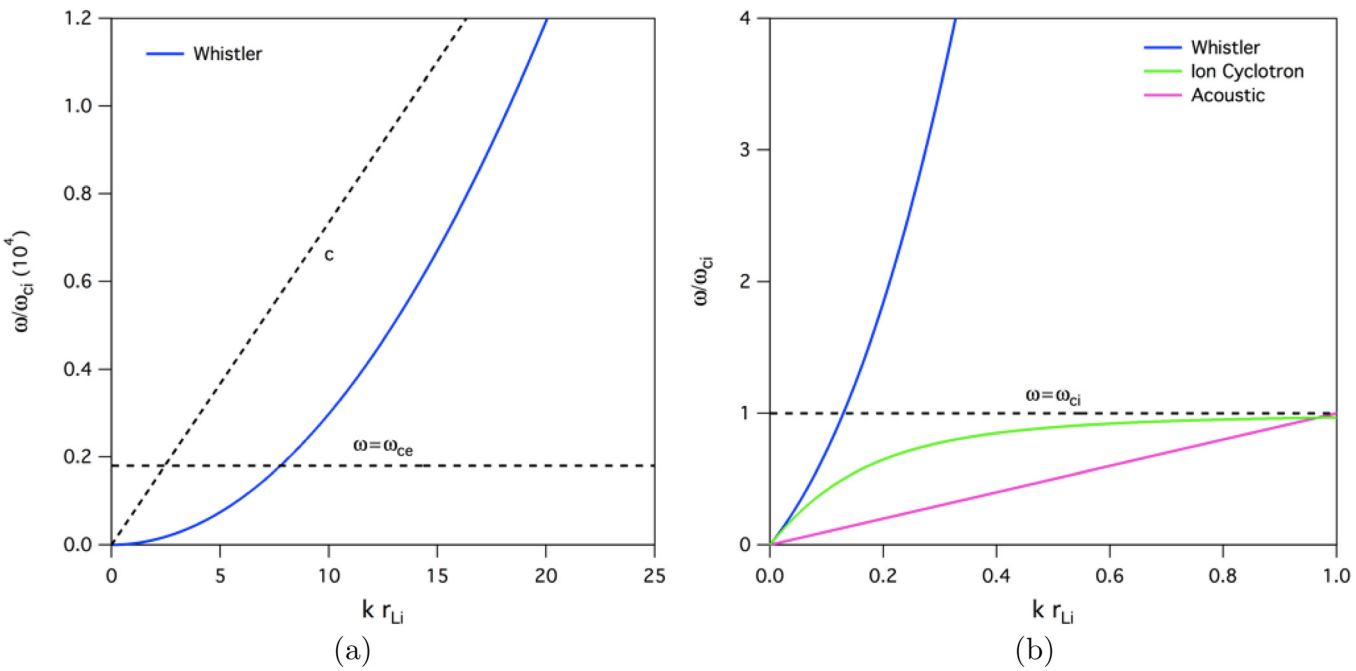

FIG. 4. (Color online) Parallel propagation dispersion relation of ω vs k when both assumptions are applied to the two-fluid plasma model, which reduces it to the Hall-MHD model. Plot (a) shows that the whistler wave frequency grows quadratically without bound as k is increased. Plot (b) has an expanded scale to show the whistler wave, the ion cyclotron wave, and the ion acoustic wave.

Figure 5 compares the whistler wave of the two-fluid plasma model, Hall-MHD, and the asymptotic model that contains electron inertia but assumes infinite speed of light. Neglecting the electron inertia generates the unbounded whistler wave and retaining finite electron inertia causes the whistler wave to asymptote at the resonance at the electron cyclotron frequency, ω_{ce}. This unbounded whistler wave speed is problematic for simulations that use the Hall-MHD model because waves with higher speeds need to be resolved as the wave number increases. This requires smaller time steps in order to resolve the two-fluid physics and, hence, longer simulation times. The explicit time step for Hall-MHD is described by

$$\Delta t = \min\left(\mathrm{CFL}\frac{\Delta x}{v_W}, \mathrm{CFL}\frac{\Delta x}{v_M}, \mathrm{CFL}\frac{\Delta x}{v_H}, \frac{0.1}{\omega_{ci}}\right), \tag{32}$$

where

$$v_W = \frac{kv_A^2}{\omega_{ci}}, v_M = \sqrt{v_A^2 + c_{si}^2}, v_H = -\frac{J}{nq}, \tag{33}$$

where CFL is the Courant-Friedrichs-Lewy condition, v_W is the whistler velocity, v_M is the magnetosonic velocity, and v_H is the Hall velocity. J is the magnitude of the total current. To compute the fastest whistler wave speed, k is chosen to be the maximum resolved by the grid scale, $k = \pi/\Delta x$.

In order to overcome the grid scale dependence of the whistler wave, a cutoff frequency is chosen such that any phenomena occurring at higher frequencies are not resolved. This does not lead to an asymptote for the whistler wave like with the two-fluid plasma model. Instead, it just cuts-off the dispersion relation above the specified wave number. This is done by employing a hyper-resistivity[17] which is included strictly for numerical reasons. The generalized Ohm's law is modified such that

$$n_e e\mathbf{E} = \mathbf{J}_e \times \mathbf{B} - \nabla p_e - \nu\nabla^2\mathbf{J}, \tag{34}$$

where ν is the hyper-resistivity parameter, which is most often held constant through all space and time. Hyper-resistivity introduces a diffusive time-scale that limits the explicit time step,

$$\Delta t < \frac{\Delta x^2}{2.0\nu}. \tag{35}$$

The Hall-MHD model does not include electron inertia, so it does not describe electron demagnetization. However, it does apply to regimes where the Larmor radius is much smaller or much larger than the scale length of interest.

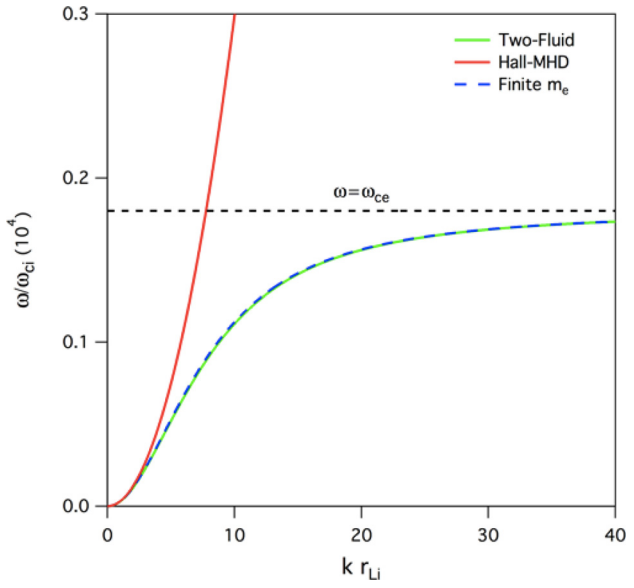

FIG. 5. (Color online) The whistler waves of the two-fluid plasma model, the Hall-MHD model, and a reduced plasma model with infinite light speed and finite electron inertia are compared. Finite electron inertia allows the whistler wave to have an asymptote at the electron cyclotron frequency whereas ignoring electron inertia causes it to grow without bound as seen in the Hall-MHD model.

IV. NUMERICAL METHOD

The simulations presented here use the Runge-Kutta discontinuous Galerkin (RKDG) method[18] in the WARPX code. A 3rd order total variation diminishing Runge-Kutta method is used for the time integration.[19] The time step is restricted for numerical stability, CFL $\leq 1/(2p-1)$, where CFL is the Courant number and p is the spatial order of the selected Legendre polynomial basis functions.[20] A spatial order of 2 is chosen for all the simulations presented here. The RKDG method is chosen for its ability to capture strong shocks by solving a Riemann problem at each cell interface, which allows the solution to be discontinuous at each cell interface. Limiters are used to reduce oscillations from developing in regions of sharp gradients. Loverich and Shumlak describe the implementation of the RKDG method for the full two-fluid plasma model.[21]

For the Hall-MHD model implementation, auxiliary state variables are introduced for $\mathbf{J}_e$ and $\mathbf{E}$ and are defined with the same discontinuous Galerkin implementation. This allows the second order derivatives to be treated consistently with a flux-source formulation similar to the first order derivatives. If hyper-resistivity is included, the $\nu\nabla^2\mathbf{J}$ term in Eq. (34) is also described as an auxiliary state variable.

V. APPLICATIONS

The full two-fluid plasma model and the Hall-MHD model are applied to several problems to study the physics captured and the ease of implementation of these models. Both models have stringent time step restrictions as described in Secs. II and III C with the explicit time-integration scheme.

To provide a physical context, $v_W = V_A$ for small k, $c \approx 10^3$–$10^4 v_A$, and $v_W \approx 10 v_A$ in some astrophysical plasmas.[22,23] For the two-fluid plasma model, c can be artificially reduced provided it is much higher than the next fastest characteristic speed in the system. In some Hall-MHD simulations, the whistler wave speed is unphysically larger than the Alfvén speed due to the nature of the Hall-MHD dispersion relation where the whistler wave frequency grows quadratically without bound as the wave number is increased. Hyper-resistivity is used to address this issue. The full two-fluid

model does not require numerical damping as long as all the temporal scales are resolved since none of the waves grow unbounded.

A. 1D electromagnetic plasma shock

A 1D electromagnetic plasma shock is initialized with a discontinuous jump at $x=0.5$ in electron and ion densities and pressures, and in the transverse magnetic field, B_z, for the two-fluid plasma model. The domain size is from $x=0$ to $x=1$ with open boundary conditions at the lower and upper boundaries. A uniform longitudinal magnetic field, B_x, is also initialized. The initial conditions used are the same as those described by Shumlak and Loverich.[1] For the Hall-MHD model, the ion density, ion and electron pressures, and magnetic fields are initialized the same as the full two-fluid case. The simulations are performed using 256 cells. The MHD limit has a zero ion Larmor radius, $r_{Li}/L=0$ where $L=1$ is the domain length.

Figures 6, 7, and 8 show solutions using the Hall-MHD model and two-fluid plasma model with different ion Larmor radii and different ion-to-electron mass ratios, $M \equiv m_i/m_e$. At an ion Larmor radius of $r_{Li}/L=0.7$ in Fig. 6, the two-fluid model using a realistic ion-to-electron mass ratio of $M=1836$ agrees well with the Hall-MHD model that assumes $M=\infty$. Even at $M=100$, the solutions agree well in regions of the rarefaction, contact discontinuity, and shock. Differences arise in the whistler wave propagation to the left of the domain. With $r_{Li}/L=0.07$ in Fig. 7, the two-fluid plasma model becomes stiff if $M=1836$ is used, because the electron plasma frequency needs to be resolved and can be more restrictive than the speed of light for setting the time step. The r_{Li} parameter is modified by changing the normalized charge, q_i, and M. r_{Li} is decreased by increasing q_i which consequently increases ω_{pi} and ω_{pe}. For high M and small r_{Li}, i.e., small q_i, ω_{pe} becomes very large. This provides a large contribution from the source terms as opposed to the fluxes, making the equation system stiff. However, artificially decreasing M in the two-fluid plasma model still

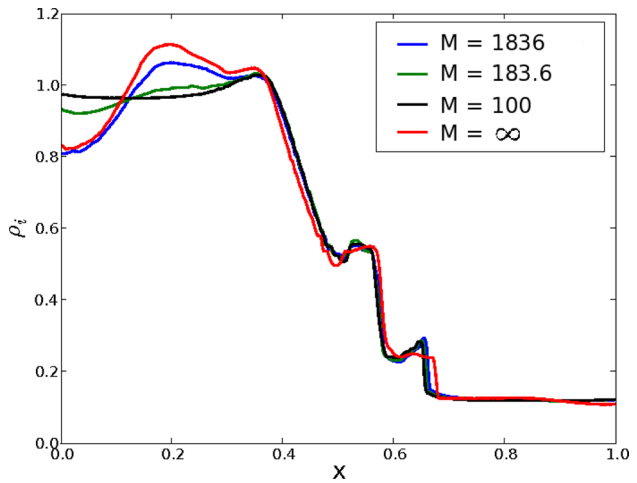

FIG. 6. (Color online) The full two-fluid plasma model and Hall-MHD results of ion density are presented after 0.2 Alfvén transit times for $r_{Li}/L=0.7$. $M=\infty$ corresponds to Hall-MHD. No hyper-resistivity is used for Hall-MHD in this plot.

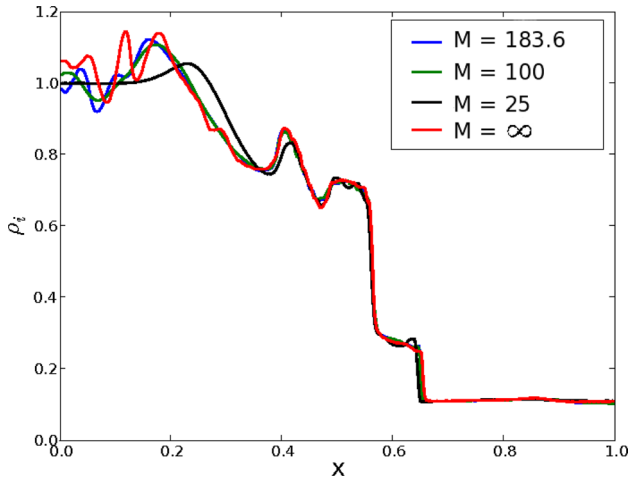

FIG. 7. (Color online) The full two-fluid plasma model and Hall-MHD results of ion density are presented after 0.2 Alfvén transit times for $r_{Li}/L=0.07$. $M=\infty$ corresponds to Hall-MHD. The Hall-MHD solution is similar to the two-fluid plasma model solution with ion-to-electron mass ratio, $mi/me=183.6$. The problem becomes stiff for the full two-fluid plasma model with $M=1836$ at $r_{Li}/L=0.07$. No hyper-resistivity is used for Hall-MHD in this plot.

provides a comparable solution to the Hall-MHD model for $r_{Li}/L=0.07$. Both the full two-fluid and Hall-MHD models generate solutions that approach the ideal MHD solution as $r_{Li}/L \to 0$, consistent with theory. This is seen from Fig. 8 for $r_{Li}/L=0.0007$, where several mass ratios are included for the two-fluid model to show convergence. In this regime, the two-fluid plasma model is stiff and the Hall-MHD model takes less computational effort.

The time step for the two-fluid plasma model is restricted by the speed of light which is set to $c=35v_A=110c_{si}=2.5c_{se}$ for $r_{Li}/L=0.7$. The speed of light for the two-fluid plasma model is chosen such that it is the fastest characteristic speed in the system. Since the speed of light is assumed infinite in the Hall-MHD model, the whistler wave speed restricts the time step with a cutoff wave number described previously

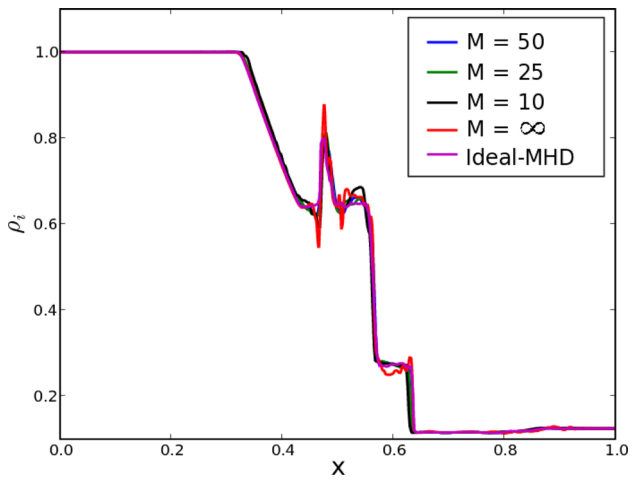

FIG. 8. (Color online) The full two-fluid plasma model, the Hall MHD model, and the ideal MHD model results of ion density are presented after 0.2 Alfvén transit times for $r_{Li}/L=0.0007$. $M=\infty$ corresponds to Hall-MHD. Solutions with decreasing r_{Li}/L approach the ideal MHD solution. No hyper-resistivity is used for Hall-MHD in this plot.

such that $v_W \approx 2275 v_A$ for this problem. However, using hyper-resistivity of $\nu \approx 10^{-6}$ leads to a $v_W \approx 227 v_A$ and the results are plotted in Fig. 9. $\upsilon \approx 10^{-6}$ is the largest value hyper-resistivity coefficient that is stable for this problem. It is noted from Fig. 9 that using hyper-resistivity does not significantly change the solution. For this problem, both the full two-fluid and Hall-MHD solutions have the same effective grid resolution. The effective grid resolution is defined as a product of the grid resolution and the spatial order chosen for the discontinuous Galerkin method.[12] The time step used for the two-fluid plasma model with $M = 1836$ and $r_{Li}/L = 0.7$ case is approximately 100 times larger than the time step used for Hall-MHD leading to 135 times more computational effort to obtain a Hall-MHD solution as compared to the two-fluid model when $\nu = 0$. With $\nu = 10^{-6}$, the computational effort is reduced to 16 times more with a 10 times larger time step for Hall-MHD as compared to the two-fluid model. For the $r_{Li}/L = 0.07$ case, the Hall-MHD model with $\nu = 0$ takes 14 times more computational effort than the $M = 183.6$ two-fluid plasma solution. Using $\nu = 10^{-6}$, Hall-MHD takes 1.6 times the computational effort of the two-fluid model. For $r_{Li}/L = 0.0007$, Hall-MHD uses less computational effort than the two-fluid plasma model which becomes stiff in this regime. However, in regimes where small spatial and temporal scales are of interest, the two-fluid plasma model uses less computational effort than the Hall-MHD model and provides accurate solutions even after artificially decreasing M and c.

Implicit implementations might overcome the large computational effort of the Hall-MHD model and the stiffness of the two-fluid plasma model presented here. The electromagnetic shock problem has strong shocks and discontinuities that need to be appropriately resolved. Numerical resistivity or hyper-resistivity that is often used with Hall-MHD introduces additional diffusion to damp the whistler wave. This diffusion also reduces the sharp physical gradients in the solution. Additionally and more importantly, implicit schemes become problematic as the solution becomes strongly nonlinear. The electromagnetic plasma shock problem is a strongly nonlinear problem and the inclusion of limiters with the RKDG scheme to reduce numerical dispersions further exacerbates the nonlinear components. As a result, implicit schemes have difficulty converging to a solution. Hence, explicit methods are presented here.

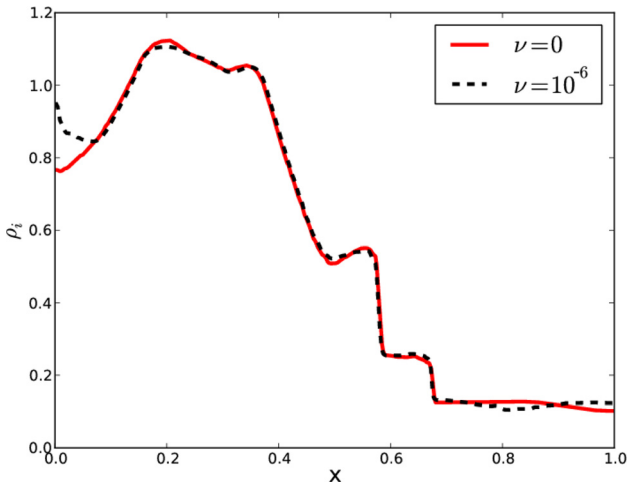

FIG. 9. (Color online) Hall-MHD results of ion density are presented after 0.2 Alfvén transit times for $r_{Li}/L = 0.7$ with and without hyper-resistivity. Without hyper-resistivity, $v_W \approx 2275 v_A$ and using a hyper-resistivity coefficient of 10^{-6} sets a cut-off wave-number for Hall-MHD such that $v_W \approx 227$ and this speeds up the computation time by a factor of 10. The artifact at $x = 0$ is caused by the diffusion of the solution from the boundary back into the domain.

B. 2D GEM challenge collisionless magnetic reconnection

Magnetic reconnection plays an important role in magnetosphere dynamics, space plasmas, and laboratory plasmas.[24,25] Collisionless magnetic reconnection results in small scale reconnection at rates that are faster than resistive reconnection.[24] Collisionless magnetic reconnection has been explored using a number of fluid and particle codes. Shay *et al.*[7] determine that the inclusion of the Hall term is necessary to produce physically correct reconnection rates, and the Hall-MHD model represents the minimum physical model needed to accurately capture collisionless magnetic reconnection.

The 2D collisionless magnetic reconnection problem is studied with the full two-fluid plasma model and the Hall-MHD model. The Hall-MHD model does not use any hyper-resistivity for this application. An out-of-plane current sheet is initialized with a current density profile of $J_z \propto \mathrm{sech}^2(y)$ and uniform in x. The current produces a magnetic field in the x direction such that $B_x \propto \tanh(y)$. A small perturbation is initialized to the magnetic field consistent with $\nabla \cdot \mathbf{B} = 0$. The electron density is initialized for the two-fluid plasma model such that it follows the current density profile. The problem domain is bounded in y by perfectly conducting walls and is periodic in x. The problem setup is the same as described in the GEM challenge.[26] Initial conditions are shown for ρ_i and B_x in Fig. 10. For the Hall-MHD model, the electron current density is calculated from the Ampere's law and the ion fluid velocity using Eq. (27). All results are for a resolution of 128×64 cells using the 2nd order RKDG method. All normalizations and parameters chosen are consistent with Ref. 26.

For the two-fluid plasma model, $M = 25$ and $c \approx 10\ v_A$ and for the Hall-MHD model, $v_W \approx 100\ v_A$. No hyper-resistivity is used for the Hall-MHD results. Figures 11 and 12 show ρ_i at a time of $\omega_{ci} t = 20$ for the two-fluid plasma model and the Hall-MHD model. Figures 11(a) and 12(a) do not include any correction of $\nabla \cdot \mathbf{B}$ errors. The effect of $\nabla \cdot \mathbf{B}$ errors is addressed later. Figures 11(b) and 12(b) include $\nabla \cdot \mathbf{B}$ corrections. Divergence corrections more accurately capture the islands that form and provide better agreement between the full two-fluid plasma and the Hall-MHD models. These islands eventually move to either side of the domain and begin to merge with the larger plasma island at a time of $\omega_{ci} t \approx 33$.

The reconnected magnetic flux for the two-fluid plasma model and the Hall-MHD model are shown in Fig. 13. The magnetic flux, Φ_{norm}, is normalized to the GEM challenge magnetic flux at $\omega_{ci} t = 0$ so the scales are the same. The reconnected flux and the reconnection rate of the two-fluid

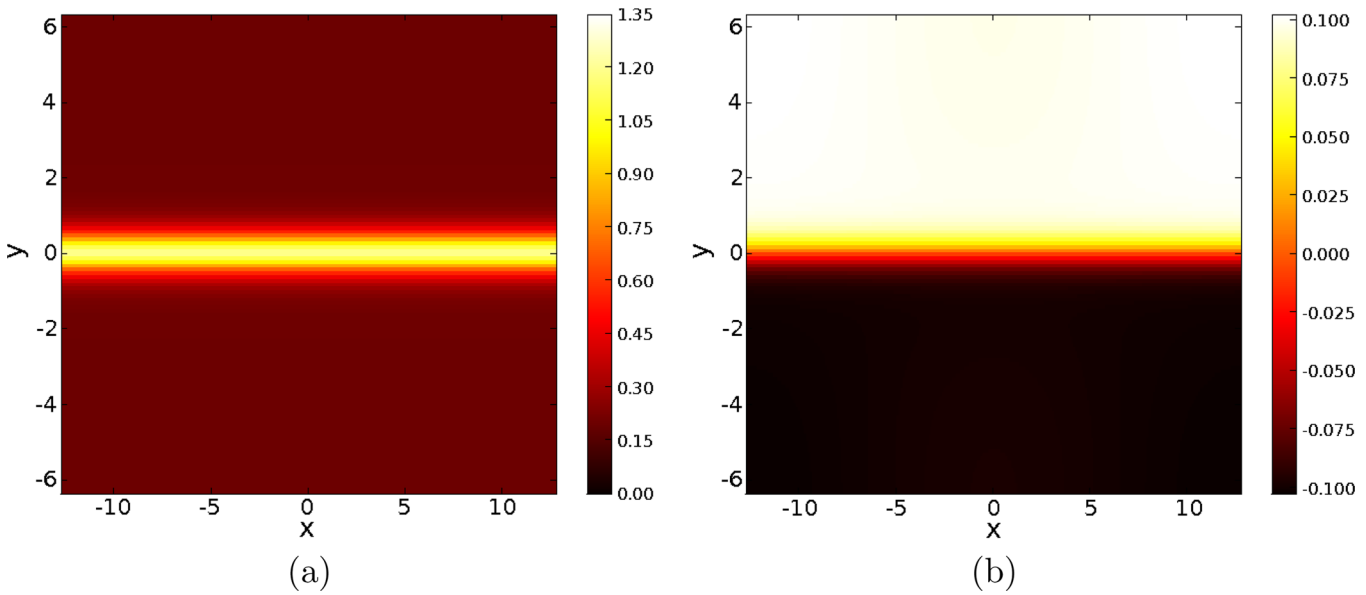

FIG. 10. (Color online) Initial conditions of (a) ρ_i and (b) B_x for the collisionless magnetic reconnection GEM challenge problem.

model do not change significantly with divergence corrections for this problem. However, the impact for the Hall-MHD model is more significant. The magnetic flux reconnection rates from this plot agree with previously published results[7] that use Hall-MHD. As described in Refs. 26 and 7, Hall-MHD reconnects more flux than hybrid and kinetic codes. The two-fluid plasma model and the $\nabla \cdot \mathbf{B}$ corrected Hall-MHD appear to saturate at approximately the same Φ_{norm} as particle solutions.

A study of divergence corrections is performed for the Hall-MHD and two-fluid plasma models to quantify the amount of error present and the correction applied. The values of the error correction coefficients were chosen such that the error correction speeds are the same as the speed of light for the full two-fluid model. For the Hall MHD model, Γ is chosen such that it equals v_W, the fastest speed in the system. This ensures that the time-step is not affected in advecting the divergence errors out of the domain. Figure 14 quantifies the $\nabla \cdot \mathbf{B}$ errors for the full two-fluid and the Hall-MHD models for this problem. The $\nabla \cdot \mathbf{B}$ errors are computed using central differencing on B_x and B_y and the values are normalized to an initial B_0/L_x, where B_0 is the initial peak magnetic field and L_x is the domain length. It is seen that the $\nabla \cdot \mathbf{B}$ errors are significantly reduced for both models when using perfectly hyperbolic Maxwell's equations divergence corrections. The reduction is more significant for the Hall-MHD model and has a correspondingly larger effect on the magnetic reconnection.

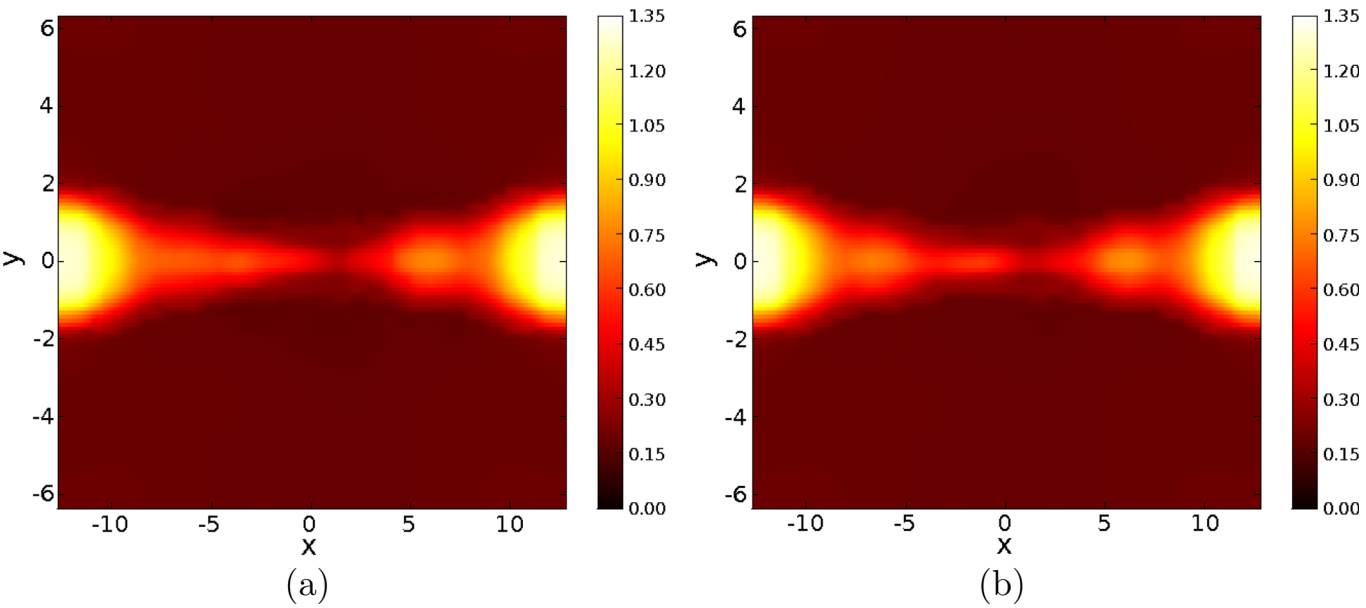

FIG. 11. (Color online) Solution of ρ_i for the full two-fluid plasma model for the magnetic reconnection problem at $\omega_{ci}t = 20$. (a) When no $\nabla \cdot \mathbf{B}$ correction is applied, an island forms in the center of the domain that moves to the right and merges with the larger plasma islands. (b) With $\nabla \cdot \mathbf{B}$ correction, two islands form in the center of the domain that move in either direction and merge with the larger plasma islands.

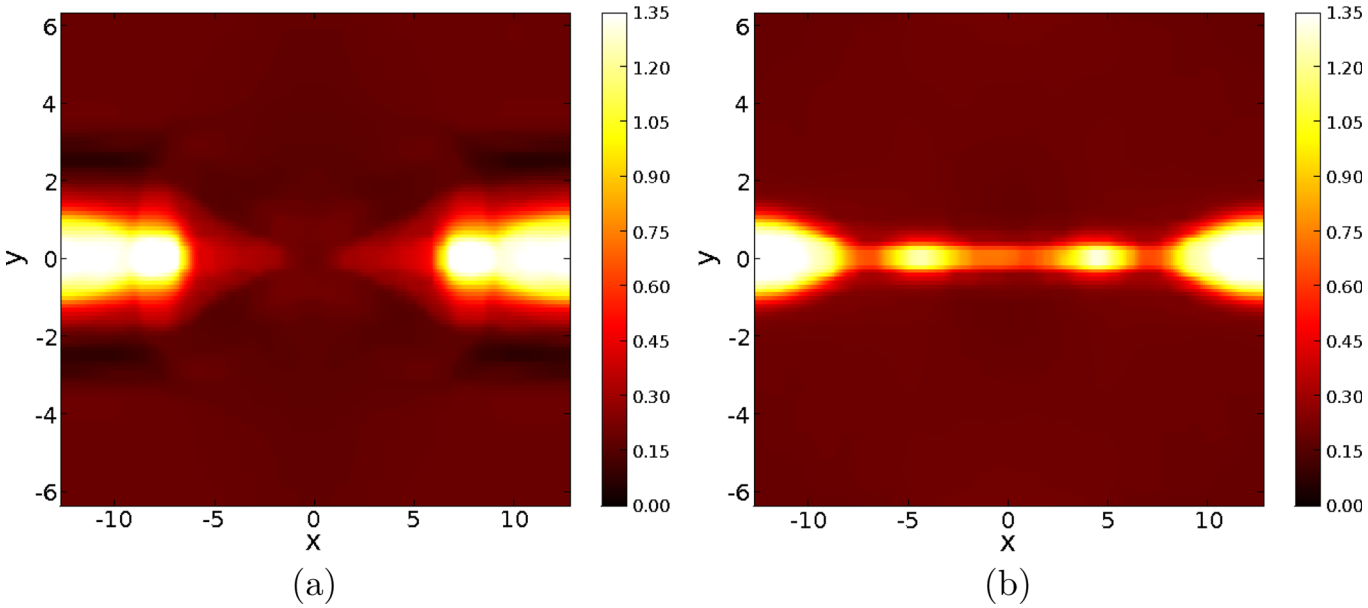

FIG. 12. (Color online) Solution of ρ_i for the Hall-MHD model for the magnetic reconnection problem at $\omega_{ci}t = 20$. (a) With no $\nabla \cdot \mathbf{B}$ correction, no noticeable island forms at the center of the domain, but an island of small magnitude appears at higher grid resolution. (b) With $\nabla \cdot \mathbf{B}$ correction, noticeable islands form at the center of the domain, then move and merge with the larger plasma islands.

The energy conservation is explored to determine how the initial magnetic energy is converted to ion and electron kinetic and thermal energies for the full two-fluid and Hall-MHD models. Figure 15 shows the variation in each of the energy components as a function of time for both fluid models. The individual components of energy are normalized to the total initial energy. It is observed that the ion thermal energy gains the largest fraction of the magnetic field energy. The electron thermal energy and ion kinetic energy also gain some of the energy from the magnetic field. The magnetic field loses about 35% of its energy to the fluids. Both fluid models provide similar results since the electron kinetic energy does not seem to grow significantly with time in the two-fluid model where electron inertia is retained. One difference is the time at which the ions gain kinetic energy from the field, which occurs at a later time for the Hall-MHD model.

For this problem, the restrictive time step of the Hall-MHD model requires 15 times the computational effort of the two-fluid plasma model. Since the reconnection rates of both models match previously published results, the two-fluid model provides the more computationally efficient solution. No explicit resistivity or dissipation is added to these models. References 7 mentions three mechanisms that break

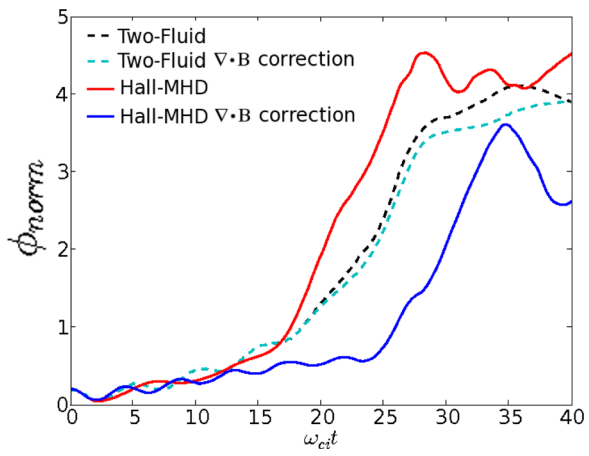

FIG. 13. (Color online) Reconnected magnetic flux is shown as a function of normalized time, $\omega_{ci}t$, for the two-fluid model (dashed lines) and Hall-MHD (solid lines) with and without divergence corrections. The solid red line is the Hall-MHD solution without $\nabla \cdot \mathbf{B}$ correction, and the solid blue line is the Hall-MHD solution with $\nabla \cdot \mathbf{B}$ correction. The dashed black line is the full two-fluid solution without $\nabla \cdot \mathbf{B}$ correction and the dashed cyan line is the full two-fluid solution with $\nabla \cdot \mathbf{B}$ correction. The magnetic flux is normalized to the GEM challenge magnetic flux at $\omega_{ci}t = 0$ so the scales are the same. The reconnection rates match well with previous literature.[7] Hall-MHD reconnects more flux than the two-fluid model before saturating when divergence corrections are not employed. The additional flux of Hall-MHD is consistent with Ref. 26.

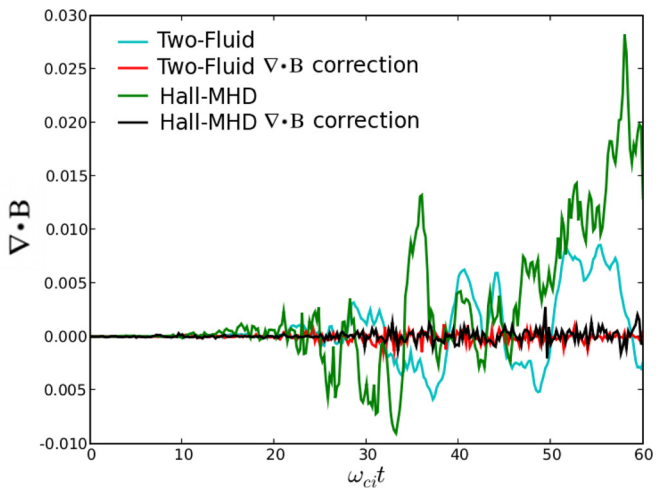

FIG. 14. (Color online) Quantifying the normalized $\nabla \cdot \mathbf{B}$ errors for the full two-fluid plasma model and for the Hall-MHD model with and without $\nabla \cdot \mathbf{B}$ corrections. It is seen that the errors are significantly reduced for both fluid models when using the perfectly hyperbolic Maxwell's equations for divergence corrections.

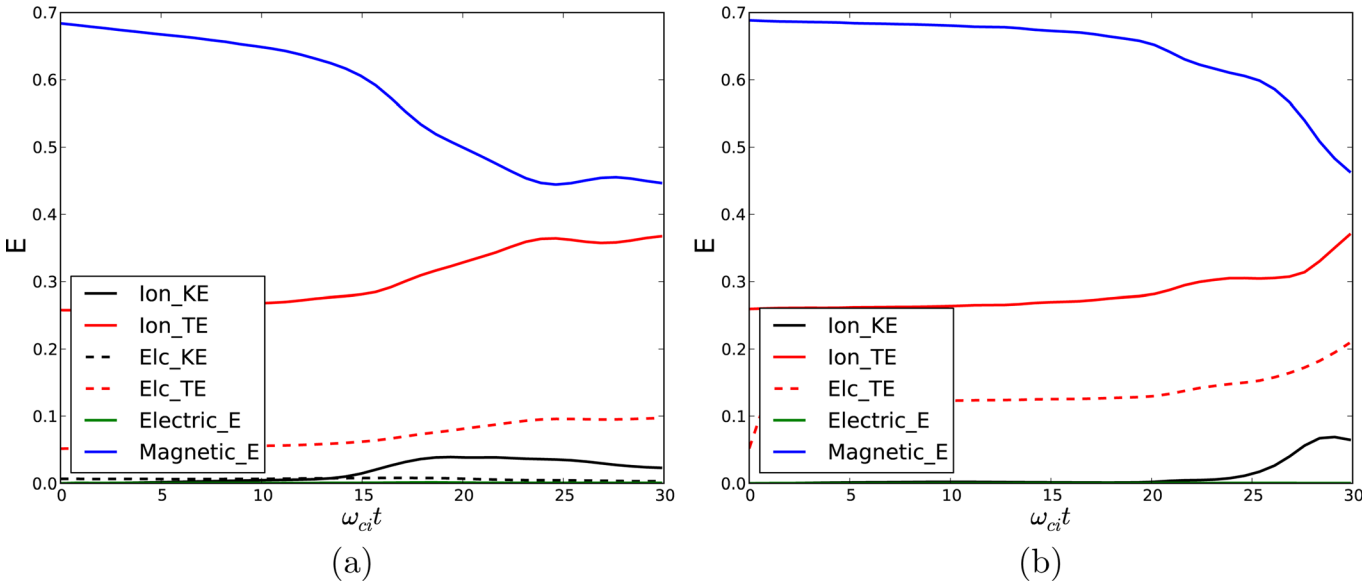

FIG. 15. (Color online) Full two-fluid (a) and Hall-MHD (b) energies plotted as a function of ion cyclotron time. Variables include ion and electron kinetic energies, ion and electron thermal energies, magnetic energy, and electric energy for each of the fluid models normalized to the total energy. All energies are normalized to the initial total energy. Due to massless electrons, there is no electron kinetic energy in Hall-MHD. Note, for both models, the magnetic energy is primarily converted to ion thermal energy as the solution evolves. The electron thermal energy and the ion kinetic energy also gain some energy from the magnetic field. The magnetic field loses about 35% of its energy to the fluids. Both fluid models provide similar results.

the frozen-in flux condition namely, electron inertia, electron thermal motion, and resistivity. For the full two-fluid plasma model, reconnection is triggered by the presence of electron inertia and electron thermal motions which break the frozen-in flux condition. The Hall-MHD model contains the electron thermal motion through the diamagnetic drift term which is represented by the gradient of the electron pressure in Eq. (26). For ideal Hall-MHD, the frozen-in flux condition seems to be broken by electron thermal motion alone. While resistivity or numerical dissipation could provide a mechanism for breaking the frozen-in law for the electrons, the results presented here do not rely on these mechanisms.

C. 2D axisymmetric Z-pinch

The drift-turbulence instability in an axisymmetric Z-pinch investigated here uses the same initial and boundary conditions presented in Refs. 2 and 12 but with a single wavelength perturbation for all plasma models. The Hall MHD model solutions are compared to the full two-fluid plasma solutions using a grid of 128×128 cells. For both models, the ratio of the pinch radius to the ion Larmor radius $r_p/r_{Li} \approx 3$. The two-fluid plasma model uses $M = 25$ and $c \approx 16v_A$. The Hall-MHD model uses $v_W \approx 400v_A$.

Figure 16 shows the formation of the short-wavelength drift-turbulence instability in the two-fluid plasma model, in ideal-MHD, and in Hall-MHD with and without hyper-resistivity. Ideal-MHD does not capture this drift-turbulence instability and forms a sausage instability based on the initial perturbation. In Fig. 16, the Hall-MHD solution is shown without any hyper-resistivity where many small-scale features are present, and with a hyper-resistivity of $\nu = 6 \times 10^{-5}$ where some of the small-scale features appear to be damped. Hyper-resistivity is applied using $\nu = 1/k^2$ where the wavenumber k is specified and maintained for all grid resolutions.

Figure 17 shows the instability growth in the magnetic field perturbation for the full two-fluid plasma model, the Hall-MHD model with $\nu = 0$, and Hall-MHD model for several values of ν. The growth rate is computed using

$$\gamma_{gr} = \int\int |\Delta \mathbf{B}| 2\pi r dr dz, \tag{36}$$

where $\Delta \mathbf{B}$ refers to the difference in magnetic field between the solutions of a perturbed equilibrium and an unperturbed equilibrium. The unperturbed equilibrium solution is needed to account for oscillations that occur in the system since the equilibrium is not a true two-fluid equilibrium initially. For $\nu = 0$, the Hall-MHD solution has a much larger initial growth rate compared to the two-fluid plasma model because of the grid scale excites shorter wavelengths of the whistler wave. For values of $\nu > 0$, the growth rate for the Hall-MHD model approaches that of the full two-fluid plasma model. The Hall-MHD model requires 35 times the computational effort of the two-fluid model for this problem with $\nu = 0$ and 8 times the computational effort when $\nu = 6 \times 10^{-5}$.

D. 2D axisymmetric FRC

An axisymmetric FRC is initialized by numerically solving the Grad-Shafranov equation to give distributions of pressure, poloidal magnetic field, and toroidal current density. The pressure is assumed to be equally distributed between ion and electron pressures, $p_i = p_e = p/2$. The density and temperature are specified assuming an adiabatic condition with $\gamma = \frac{5}{3}$ such that

$$n_s = \frac{1}{k} p_s^{1/\gamma}, \tag{37}$$

$$T_s = p_s^{(\gamma-1)/\gamma}, \tag{38}$$

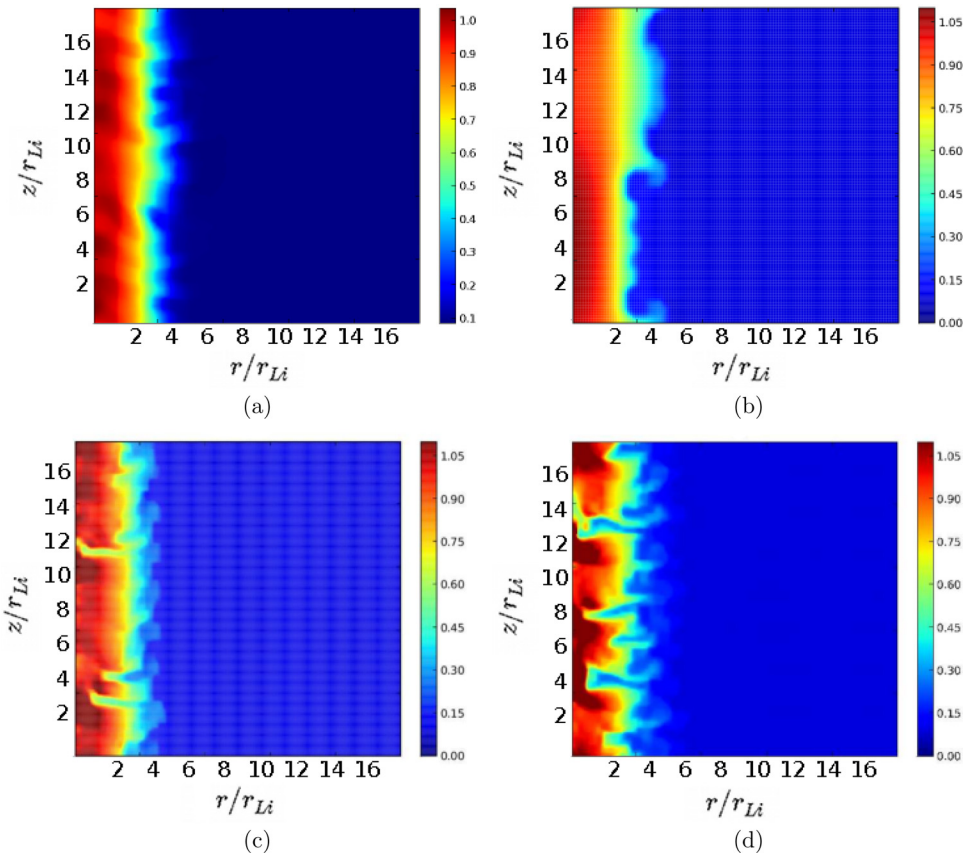

FIG. 16. (Color online) Ion density after 1.5 Alfvén transit times for the axisymmetric Z-pinch using (a) the full two-fluid plasma model, (b) the ideal MHD model solution, (c) the Hall-MHD model with $\nu = 0$, (d) the Hall-MHD model with $\nu = 6.5 \times 10^{-5}$. For the same single wavelength perturbation, a small-scale, drift-turbulence instability grows for the two-fluid plasma and the Hall-MHD solutions whereas the ideal MHD solution just forms the single-wavelength sausage instability.

where n_s is the species number density, T_s is the species temperature, p_s is the species pressure, and k is the Boltzmann constant. The azimuthal current that results from the equilibrium is initialized as electron current. The evolution of the equilibrium is studied using the full two-fluid plasma model and the Hall-MHD model. Figure 18 shows the initial total fluid pressure and the initial electron current with vector plots of the magnetic fields superimposed. The simulations presented here have a resolution of 64×64 cells with a spatial order of 2 for both the full two-fluid plasma model and the Hall-MHD model. Axis boundary conditions are implemented at $r/r_{Li} = 0$ and conducting wall boundary conditions are implemented at $r/r_{Li} = 115$. Periodic boundary conditions are implemented in the axial direction instead of open boundaries to prevent artificial reflections from affecting the equilibrium profile, particularly in the magnetic fields at the domain edges. The kinetic parameter, s, which is the ratio of the separatrix radius to the ion skin depth, is approximately 20. For the full two-fluid plasma model, $c \approx 8v_A$ and $M = 25$. For the Hall-MHD model, $v_W \approx v_A$ which is the result of the MHD equilibrium having $\delta_i \ll L$. Since the equilibrium is initially in the MHD regime, the Hall-MHD model is more computationally efficient because $r_{Li} \ll L$ and $\delta_i \ll L$ which results in the full two-fluid plasma model being stiff.

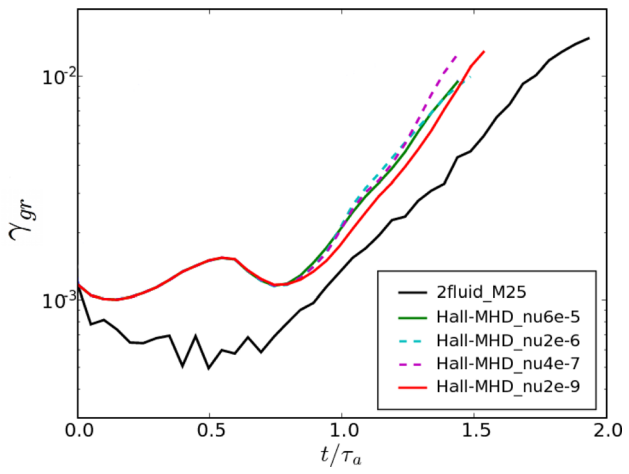

FIG. 17. (Color online) Growth of the magnetic field perturbation as a function of normalized time, t/τ_a, where τ_a is the Alfvén transit time when using a single wavelength perturbation. Notice that with increasing dissipation, the growth rate for the Hall-MHD solutions approach that of the two-fluid plasma solution.

Two-fluid plasma models are important to study FRC physics. FRC experiments have observed the self-generation of toroidal magnetic fields,[27,28] which can be large during FRC formation and become smaller once a stationary equilibrium is achieved. The ideal MHD model without Hall effects does not allow the self-generation of toroidal magnetic fields in FRCs and maintains the equilibrium of Fig. 18 unchanged in the axisymmetric simulations performed here. Two-fluid plasma models, however, allow spontaneous generation of toroidal magnetic fields and toroidal velocities[29] due to the inclusion of the diamagnetic drift term and the Hall term.[30]

Consistent with Ref. 29, Figs. 19 and 20 for the full two-fluid plasma and Hall-MHD solutions after $5t_A$ and $10t_A$

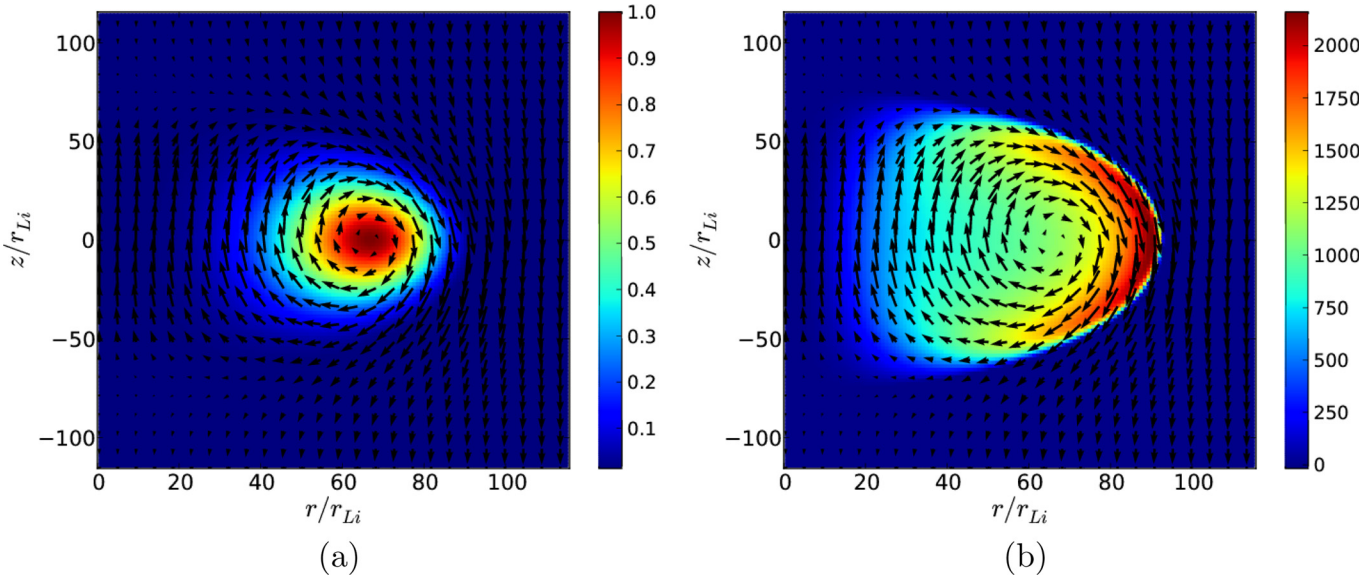

FIG. 18. (Color online) Initial condition for an axisymmetric FRC using an MHD equilibrium. (a) Contours of the total pressure with the magnetic field vectors normalized to the pressure at the separatrix. (b) Contours of azimuthal current density with magnetic field vectors.

show the spontaneous generation of a toroidal field with equal and opposite magnitudes on each side of the axial plane to maintain zero net toroidal flux. The toroidal magnetic fields have only a small effect on the equilibrium configuration. The Hall term produces the toroidal magnetic field by causing the field lines to be frozen to the electron fluid instead of the ion fluid. Reference 29 explains that the toroidal field results because of the poloidal field lines being frozen to the electron fluid while the electron toroidal velocity varies along the field lines.

Figures 19 and 20 show that the toroidal magnetic fields after $5t_A$ and $10t_A$ are approximately an order of magnitude larger in the full two-fluid plasma model as compared to the Hall-MHD model. For the full two-fluid plasma model, the toroidal magnetic fields are between 1% and 5% of the poloidal magnetic fields. The two-fluid model contains additional terms besides the diamagnetic drift and the Hall term that break the frozen-in-flux condition. These include the temporal and spatial derivatives that result from including finite electron inertia. An asymptotic study of the total fluid pressure for different mass ratios $M=50$ and $M=100$ in Fig. 21 after $5t_A$ shows that the full two-fluid solution is not affected by the artificial ion-to-electron mass ratio. The magnitudes of the observed toroidal magnetic fields are comparable to $M=25$ in Fig. 19.

Neither the full two-fluid plasma model nor the Hall-MHD model contains any explicit resistivity for the FRC simulations. An effective resistivity is measured for both models using

$$\eta = \int \frac{\mathbf{E}\cdot\mathbf{j}}{\mathbf{j}\cdot\mathbf{j}} dV. \tag{39}$$

The effective resistivity observed for the full two-fluid plasma model is significantly larger than the Hall-MHD effective resistivity and the Spitzer resistivity calculated for the same simulation parameters. The comparison is shown in Fig. 22. Figure 23 shows the net toroidal magnetic field normalized to the peak poloidal magnetic field in the full two-fluid plasma model and in Hall-MHD. It is noted that the net toroidal magnetic field is very small for both fluid models and this could be due to numerical errors.

VI. DISCUSSION

The full two-fluid plasma model is explored and asymptotic approximations are applied to obtain the Hall-MHD model. The two-fluid plasma model and the Hall-MHD model retain the two-fluid physics by including the Hall and diamagnetic-drift terms that are neglected in the single fluid MHD plasma models. The full two-fluid plasma model is implemented as a set of hyperbolic balance laws, which are solved using an RKDG method. The electromagnetic shock shows slight differences between the full two-fluid plasma model and the Hall-MHD model that result from including finite electron inertia. For the Z-pinch two-fluid drift-turbulence instability, the Hall-MHD model requires a hyper-resistivity to predict a consistent growth rate. For the FRC, the toroidal magnetic field and the effective resistivity are significantly larger in the full two-fluid plasma model (while the net toroidal magnetic fields are close to 0) as compared to the Hall-MHD model in the absence of any explicit resistivity.

The two-fluid plasma model is different from the more commonly used Hall-MHD model in three specific ways. The two-fluid plasma model includes

- finite electron mass,
- finite speed of light, and
- non-neutral effects.

Retaining the electron inertia allows the whistler wave to asymptote at a resonance of the electron cyclotron frequency, which is a physically correct behavior, and this allows for simpler computations. Since the asymptote for the

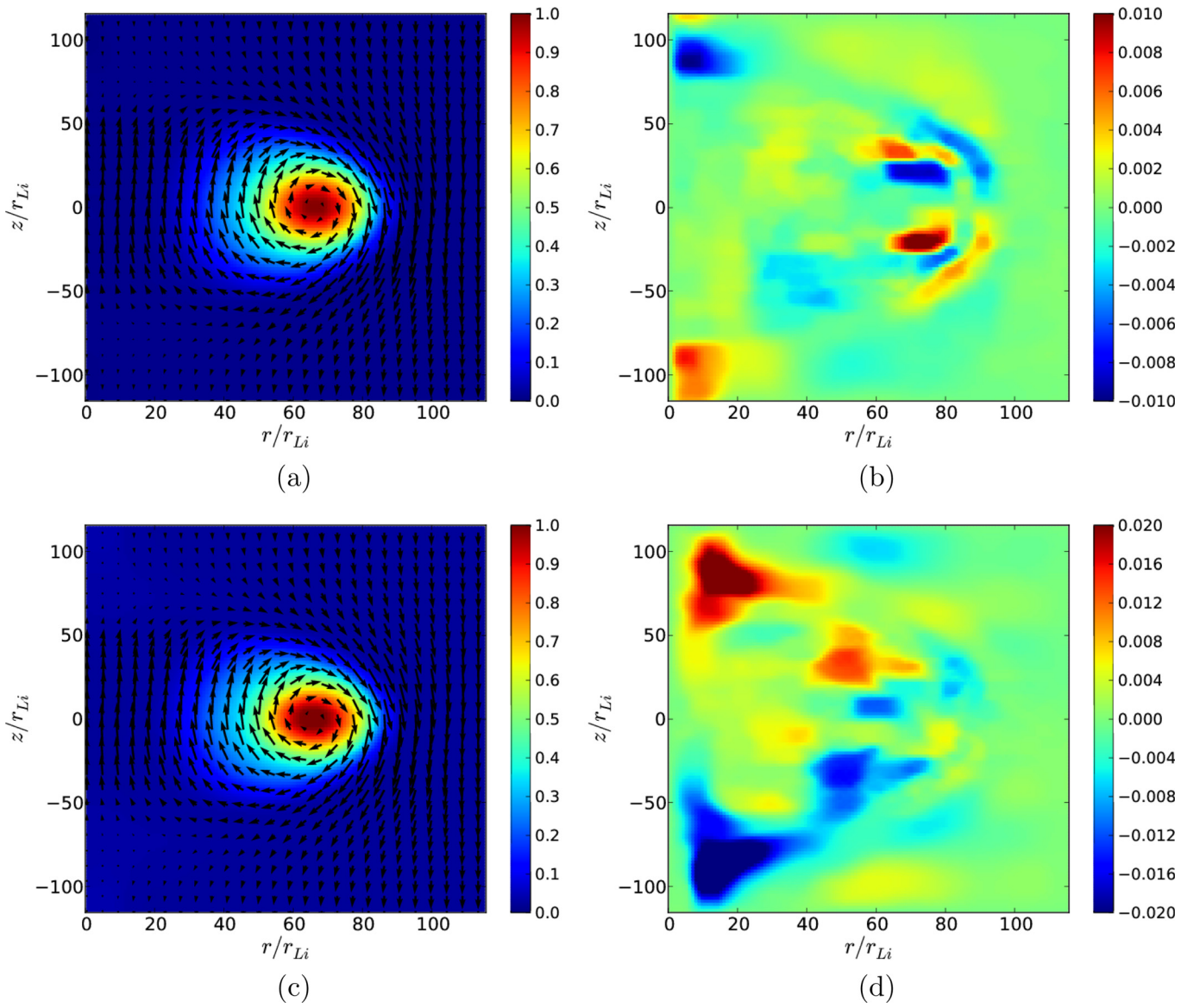

FIG. 19. (Color online) (a) Total fluid pressure with poloidal magnetic field vectors superimposed after $5t_A$. (b) Toroidal magnetic field after $5t_A$ for the full two-fluid plasma model. (c) Total fluid pressure with poloidal magnetic field vectors superimposed after $10t_A$. (d) Toroidal magnetic field after $10t_A$ for the full two-fluid plasma model. Note the formation of toroidal magnetic field as the solution relaxes to a two-fluid equilibrium.

whistler wave now lies at the electron plasma frequency, there is no need to set an artificial resistivity or hyper-resistivity to choose a cutoff frequency for the whistler wave. The whistler wave in the Hall-MHD model can be problematic since it is unbounded, and numerical diffusion must be added to cut off high frequency phenomena.

Retaining a finite speed of light in Maxwell's equations allows displacement currents to be captured in the system. The effect is relevant even for non-relativistic simulations since the interest lies in capturing the physics associated with the ion and electron fluids. Electromagnetic waves can be captured without including relativistic effects and having waves in the system that propagate at speeds close to the speed of light does not require relativistic effects. Relativistic effects are important if the fluid motions occur at time-scales approaching those associated with the speed of light, which is not the case for the simulations presented here. The fluid physics at the high frequency electromagnetic time scales is not presently of interest for the applications concerned here.

In most plasma fluid models, a parallel electric field cannot exist unless there is a resistivity included in the equation system. In this context, parallel and perpendicular are in relation to the magnetic field. To elaborate, the generalized Ohm's law for an ideal plasma, $\mathbf{E} = -\mathbf{u}_i \times \mathbf{B}$, does not allow for a parallel electric field unless an $\eta \mathbf{J}$ term is also included. This implies that in most reduced fluid models, a parallel electric field can exist only if there is a parallel current and resistivity. In the two-fluid plasma model, including Ampere's law with the displacement current allows a parallel electric field to be present self-consistently even without a parallel current. Even for the idealized two-fluid model presented here, i.e., no explicit resistivity, a parallel electric field can exist and is captured in the model.

Including the speed of light and consequently the displacement currents allows for local non-neutral effects to be

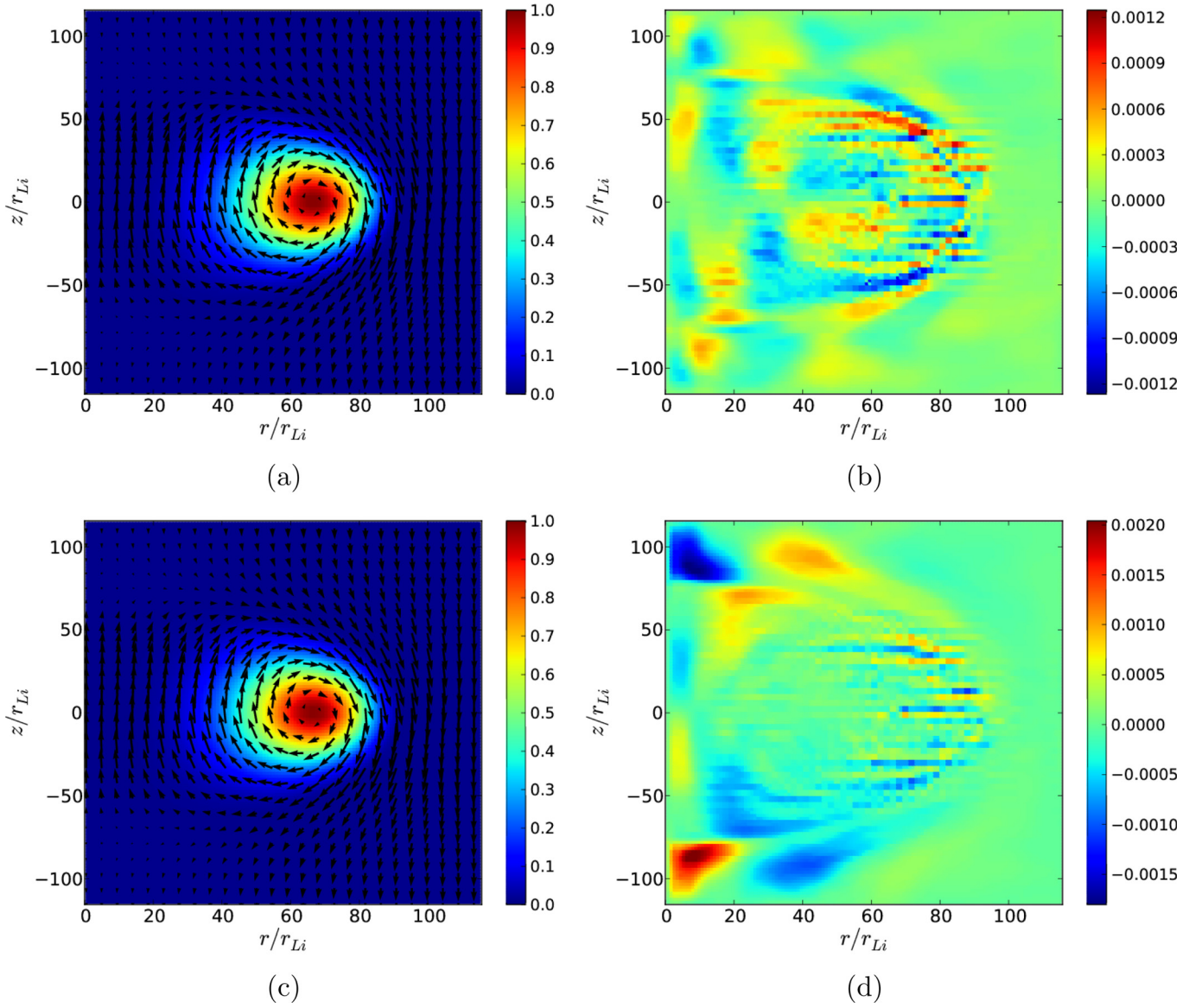

FIG. 20. (Color online) (a) Total fluid pressure with poloidal magnetic field vectors superimposed after $5t_A$. (b) Toroidal magnetic field after $5t_A$ for the Hall-MHD model. (c) Total fluid pressure with poloidal magnetic field vectors superimposed after $10t_A$. (d) Toroidal magnetic field after $10t_A$ for the Hall-MHD model. The pixelation in the magnetic field is a result of not numerically limiting the auxiliary electric field that is used in Faraday's law. Note that the toroidal magnetic fields that form are about an order of magnitude smaller than the full two-fluid solution in Fig. 19.

captured in the plasma. Single fluid MHD and even Hall-MHD models do not capture local non-neutral effects. Charge neutrality is an inherent assumption of the Hall-MHD model. The charge neutrality assumption does not allow local charge separation as a result of which potentially large local electric fields are missed. Non-neutral effects can

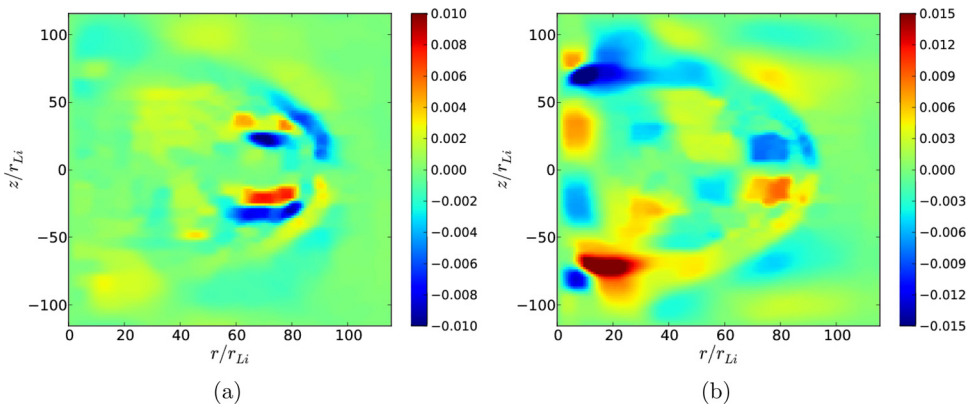

FIG. 21. (Color online) Toroidal magnetic field for full two-fluid plasma model (a) with $M = 50$ and (b) with $M = 100$ after $5t_A$. Note that the solution magnitudes are of the same order as the $M = 25$ full two-fluid solution in Fig. 19.

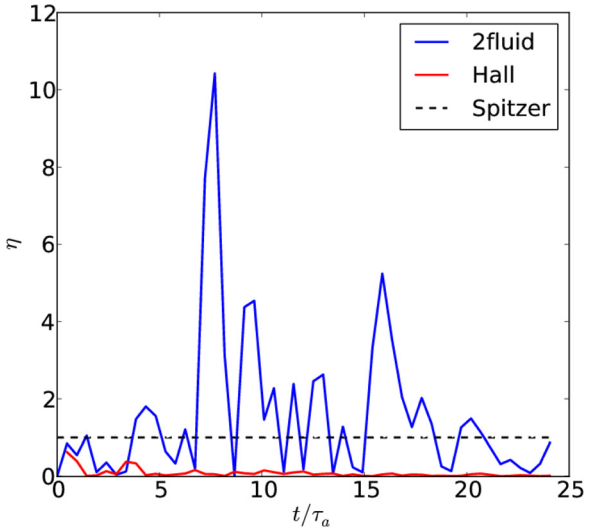

FIG. 22. (Color online) An effective resistivity, η, observed for the full two-fluid plasma model as compared to the Hall-MHD model and Spitzer resistivity. The full two-fluid effective resistivity is significantly larger. The resistivities are normalized to the Spitzer resistivity for this regime.

be important in plasmas and the full two-fluid plasma model is required to capture them. Even with the ideal full two-fluid plasma model, an effective resistivity can be observed[4] which likely results from non-neutral effects. The effective resistivity observed in Hall-MHD is much smaller in magnitude compared to that of the two-fluid plasma model.

Semi-implicit solvers have been implemented for Hall-MHD with special treatment for just the Hall term such that the remaining MHD terms are advanced at the single fluid time-scales. Examples of these are the implicit treatment of the Hall term[31] and explicit sub-cycling of just the Hall term using smaller time-steps[6] with explicit treatment of the remaining MHD terms at single-fluid time-scales. A semi-implicit Hall-MHD scheme with adaptive mesh refinement has been implemented in previous publications.[32] Chacón and Knoll propose a fully implicit Hall-MHD scheme with physics-based preconditioning.[33] In solving the full two-fluid plasma model, similar techniques can be used for implicit treatment or explicit sub-cycling of just the electron and Maxwell's equations while explicitly solving the ion equations. However, implicit schemes can have convergence issues as shocks develop and as the solution becomes strongly nonlinear. The presence of limiters exacerbates this problem. The explicit full two-fluid plasma model presented here captures shocks and sharp gradients without the need for numerical damping of high frequency waves. Two-fluid physics is captured for problems with sharp gradients with reasonable computational effort by artificially decreasing the ion-to-electron mass ratio and the light-to-Alfvén speed ratio using the full two-fluid plasma model.

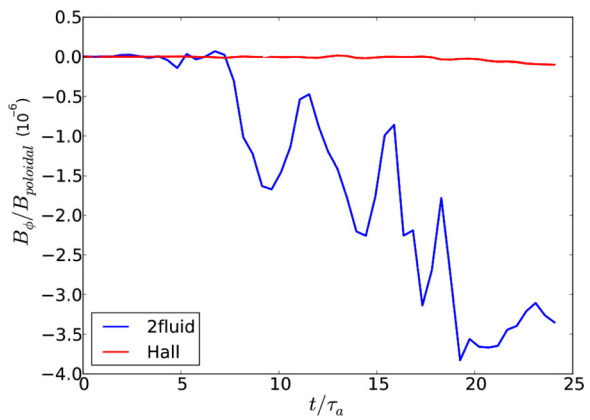

FIG. 23. (Color online) The net toroidal magnetic field, B_φ, normalized to the peak poloidal field is calculated for the full two-fluid plasma model and for the Hall-MHD model. Note that the net B_φ is very small in both fluid models and this could be attributed to numerical errors.

There are implications of the research presented here on some areas of ongoing research such as the penetration of magnetic fields into a plasma.[34–36] Small-scale density fluctuations in a plasma can drive large density gradients that can enhance the Hall electric field which is an explanation for magnetic field penetration into a plasma.[34] This draws parallels with the Z-pinch small-scale instability where the instability grows in the region of maximum density gradient. Including two-fluid effects allows small-scale spatial phenomena to be captured. The two-fluid plasma model and Hall-MHD resolve the ion skin depth and the two-fluid model also resolves the electron skin depth. References 35 and 36 explore magnetic field penetration in an initially homogeneous plasma, where resistivity determines the shock structure for high collisionality and electron inertia determines the shock structure for low collisionality. For this problem, Hall-MHD does not capture the necessary physics since it ignores electron inertia. Using the full two-fluid plasma model, magnetic field penetration requires collisions, but it may be possible to achieve a small amount of dissipation from the numerical method and limiters alone. This could provide a solution where the shock structure is determined by the electron inertia without any explicit collisions included in the model but a very low collisionality case implied as a result of the numerical method. This problem is an example of an interesting application that would require the full two-fluid plasma model over Hall-MHD.

ACKNOWLEDGMENTS

The work presented in this paper was supported by AFOSR Grant No. FA9550-09-1-0135. The authors wish to thank Dr. Ammar Hakim and Dr. John Loverich for helpful discussions that enabled the discontinuous Galerkin method and Hall-MHD to be successfully implemented and benchmarked in WARPX. Dr. George Marklin's equilibrium solver was used to specify a numerical equilibrium for the FRC. The use of the ICE cluster at the University of Washington and the MANA cluster at the Maui High Performance Computing Center are gratefully acknowledged.

[1]U. Shumlak and J. Loverich, J. Comput. Phys. **187**, 620 (2003).
[2]J. Loverich and U. Shumlak, Phys. Plasmas **13**, 082310 (2006).
[3]A. Hakim, J. Loverich, and U. Shumlak, J. Comput. Phys. **219**, 418 (2006).
[4]A. Hakim and U. Shumlak, Phys. Plasmas **14**, 055911 (2007).
[5]S. Baboolal and R. Bharuthram, Math. Comput. Simul. **76**, 3 (2007).
[6]J. Huba, "Hall-magnetohydrodynamics—A tutorial," in *Space Plasma Simulations* (Springer, Berlin, 2003).
[7]M. Shay, J. Drake, B. Rogers, and R. Denton, J. Geophys. Res. **106**, 3759, doi:10.1029/1999JA001007 (2001).

[8]J. Huba, Phys. Rev. Lett. **72**, 2033 (1994).
[9]A. Otto, J. Geophys. Res. **106**, 3751, doi:10.1029/1999JA001005 (2001).
[10]J. P. Friedberg, *Ideal Magnetohydrodynamics* (Plenum, New York, 1987).
[11]U. Shumlak, R. Lilly, N. Reddell, E. Sousa, and B. Srinivasan, Comput. Phys. Commun. **182**, 1767 (2011).
[12]B. Srinivasan, A. Hakim, and U. Shumlak, Commun. Comput. Phys. **10**, 183 (2011).
[13]C.-D. Munz, P. Omnes, R. Schneider, E. Sonnendrücker, and U. Voß, J. Comput. Phys. **161**, 484 (2000).
[14]P. Banks, W. Edwards, C. Rasmussen, and R. Thompson, Geophys. Res. Lett. **8**, 95, doi: 10.1029/GL008i001p00095 (1981).
[15]A. Dedner, F. Kemm, D. Kröner, C.-D. Munz, T. Schnitzer, and M. Wesenberg, J. Comput. Phys. **175**, 645 (2002).
[16]S. Ohsaki and S. Mahajan, Phys. Plasmas **11**, 898 (2004).
[17]R. Fitzpatrick, Phys. Plasmas **11**, 937 (2004).
[18]B. Cockburn, G. Karniadakis, and C.-W. Shu, "The development of discontinuous Galerkin methods," in *Discontinuous Galerkin Methods: Theory, Computation and Applications. Lecture Notes in Computational Science and Engineering* (Springer, Berlin/Heidelberg, 2000), Vol. 11.
[19]C.-W. Shu, SIAM J. Sci. Stat. Comput. **9**, 1073 (1988).
[20]B. Cockburn and C.-W. Shu, J. Sci. Comput. **16**, 173 (2001).
[21]J. Loverich, A. Hakim, and U. Shumlak, Commun. Comput. Phys. **9**, 240 (2011).
[22]M. Stix, *The Sun* (Springer-Verlag, Heidelberg, 1991).
[23]F. Chen, *Introduction to Plasma Physics and Controlled Fusion* (Plenum, New York, 1984).
[24]E. Priest and T. Forbes, *Magnetic Reconnection: MHD Theory and Applications* (Cambridge University Press, New York, 2000).
[25]D. Biskamp, *Magnetic Reconnection in Plasmas* (Cambridge University Press, Cambridge, 2000).
[26]J. Birn, J. Drake, M. Shay, B. Rogers, R. Denton, M. Hesse, M. Kuznetsova, Z. Ma, A. Bhattacharjee, and A. Otto, J. Geophys. Res. **106**, 3715, doi: 10.1029/1999JA900449 (2001).
[27]M. Tuszewski and B. Wright, Phys. Rev. Lett. **63**, 2236 (1989).
[28]A. Shiokawa, S. Okada, Y. Ito, and S. Goto, Jpn J. Appl. Phys. **30**, 1142 (1991).
[29]R. Milroy and J. Brackbill, Phys. Fluids **4**, 1184 (1986).
[30]D. Hewett, Nuclear Fusion **24**, 349 (1984).
[31]D. Harned and Z. Mikić, J. Comput. Phys. **83**, 1 (1989).
[32]L. Arnold, J. Dreher, and R. Grauer, Computer Phys. Commun. **178**, 553 (2008).
[33]L. Chacón and D. Knoll, J. Comput. Phys. **188**, 573 (2003).
[34]R. Arad, K. Tsigutkin, Y. Maron, A. Fruchtman, and J. Huba, Phys. Plasmas **10**, 112 (2003).
[35]A. Fruchtman and L. Rudakov, Phys. Rev. Lett. **69**, 2070 (1992).
[36]A. Fruchtman and K. Gomberoff, Phys. Fluids B **5**, 2371 (1993).